Available online at www.sciencedirect.com

SCIENCE DIRECT®

Comput. Methods Appl. Mech. Engrg. 193 (2004) 449–468

Computer methods in applied mechanics and engineering

www.elsevier.com/locate/cma

Goal-oriented *hp*-adaptivity for elliptic problems

P. Šolín [a,*], L. Demkowicz [b]

[a] *CAAM, Rice University, MS 134, P.O. Box 1892, Houston, TX 77251, USA*

[b] *ICES, The University of Texas at Austin, Austin, TX, USA*

Received 18 December 2002; received in revised form 28 May 2003; accepted 15 September 2003

Abstract

We propose and test a fully automatic, goal-oriented *hp*-adaptive strategy for elliptic problems. The method combines two techniques: the standard goal-oriented adaptivity based on a simultaneous solution of a dual problem, and a recently proposed *hp*-strategy based on minimizing the projection-based interpolation error of a reference solution. The proposed strategy is illustrated with two numerical examples: Laplace equation in L-shape domain, and an axisymmetric Maxwell problem involving radiation of a loop antenna wrapped around a metallic cylinder into a conductive medium.

Keywords: *hp* finite elements; *hp*-adaptivity; Dual problem; Goal-oriented adaptivity

1. Introduction

Nowadays, when a solid theoretical foundation of *p*- and *hp*-adaptive finite element methods for PDEs is available (see e.g., [2,7,18] and others), an intensive research effort focusses on the development of automatic *hp*-adaptive algorithms and their efficient computer implementation. Several algorithmic realizations of automatic *hp*-adaptivity, based on various error estimation techniques, have been developed—see, e.g., [10] for a recent review. The technology of higher-order finite element methods is presented in great detail in a recent book [19].

This paper is devoted to the extension of the original energy-driven fully automatic *hp*-adaptive strategy for elliptic problems [8] to goal-oriented *hp*-adaptivity. The main advantages of the presented approach are that it does not need *any a priori information* about singularities or steep gradients of the solution for the construction of the initial mesh, and that it fully automatically delivers exponential convergence rates in the full range of error level, especially in the *preasymptotic range*. The strategy does not use any explicit error estimates to guide the *hp*-refinements—instead, an approximate error function is recovered from a suitable *reference solution*, which is an approximation of the exact solution that is substantially more accurate than the approximation on the coarse mesh. Sequence of optimal *hp*-meshes is obtained by minimizing

* Corresponding author.

0045-7825/$ - see front matter
doi:10.1016/j.cma.2003.09.015

appropriate projection-based interpolation error of the reference solution in each step. The procedure will be discussed in more detail later.

The idea of adding the solution of the dual problem to the *hp*-adaptive strategy is motivated by several practical examples, where both the energy-driven *hp*-adaptivity as well as the goal-oriented *h*-adaptivity turned out to be incapable of achieving a required accuracy. One such problem is presented in Section 2.1.

Before we bring together the goal-oriented adaptivity and *hp*-adaptivity in Section 3, we briefly review the basic principles of each of them separately in Sections 2.2 and 2.3. In Section 2.4 we describe the mesh optimization procedure which represents the most important step of the *hp*-adaptive algorithm. In Section 3.4 the performance of energy-driven and goal-oriented *h*- and *hp*-adaptive versions of the automatic *hp*-adaptive strategy from Section 3 is illustrated on a rather simple model elliptic problem (Laplace equation in the L-shape domain). Finally, in Section 4 the challenging problem from Section 2.1 is solved. Conclusions and outlook for future work are drawn in Section 5.

2. Model problem and adaptivity

We are concerned with the solution of the standard model radiation problem relevant to drilling technologies, [11]. The problem is illustrated in Fig. 1: a loop antenna, wrapped around an infinite metallic cylinder, radiates into a conductive homogeneous medium.

2.1. Maxwell's equations and FE approximations

The problem consists in solving the time-harmonic Maxwell's equations,

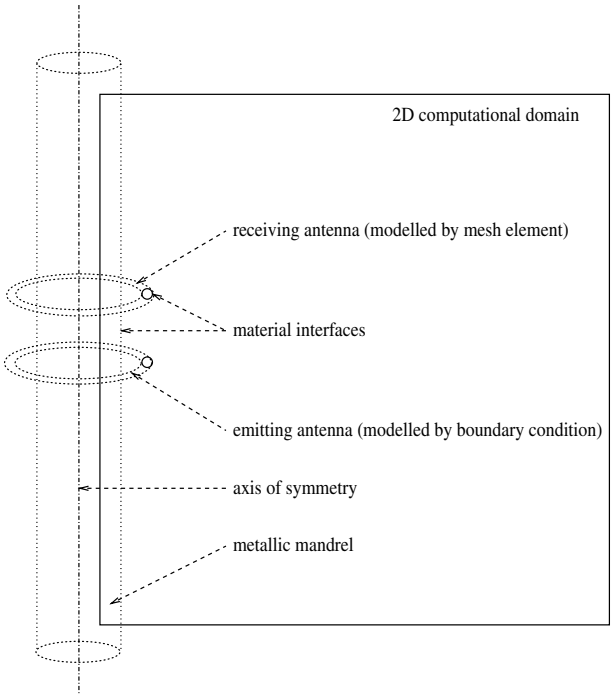

Fig. 1. Basic arrangement of the device and computational domain (with adjusted scaling in the *r*-direction). The actual measures are given later in Section 4.1.

$$\nabla \times \left(\frac{1}{\mu} \nabla \times \boldsymbol{E} \right) - (\omega^2 \epsilon - \jmath \omega \sigma) \boldsymbol{E} = 0, \tag{2.1}$$

to be satisfied in the whole space minus domain D occupied by the loop antenna, with a prescribed impressed surface current on the surface of the antenna,

$$\boldsymbol{n} \times \left(\frac{1}{\mu} \nabla \times \boldsymbol{E} \right) = -\jmath \omega \boldsymbol{J}_s^{\text{imp}}. \tag{2.2}$$

We choose to model the antenna with a surface rather than volume current (Neumann boundary condition instead of a source term) to avoid unnecessary refinements in the domain occupied by the antenna.

The standard variational formulation reads as follows [16]

$$\int_{R^3 \setminus D} \frac{1}{\mu} \nabla \times \boldsymbol{E} \cdot \nabla \times \boldsymbol{F} - \int_{\mathbf{R}^3 \setminus D} (\omega^2 \epsilon - \jmath \omega \sigma) \boldsymbol{E} \cdot \boldsymbol{F} = -\jmath \omega \int_{\partial D} \boldsymbol{J}_s^{\text{imp}} \cdot \boldsymbol{F}, \tag{2.3}$$

for every test function $\boldsymbol{F}$, with $\boldsymbol{E}$ and $\boldsymbol{F}$ satisfying appropriate boundary conditions at infinity and ∂D denoting the boundary of domain D occupied by the antenna. Two essential simplifications can be made:

- Due to the axisymmetry of the problem, components $E_r = E_z = 0$ and $E = E_\varphi = E_\varphi(r, z)$ (in the sequel we leave out the index φ for tangential component of $\boldsymbol{E}$).
- Due to the exponential decay of the solution away from the antenna, the resulting two-dimensional problem for E can be stated in a bounded rectangular domain Ω shown in Fig. 1, encompassing a portion of the metallic mandrel terminated away from $r = 0$. The equation is accompanied with a homogeneous Dirichlet boundary condition on the truncating boundary Γ.

The ultimate 2D variational problem, stated in polar coordinates (r, z) reads as follows:

$$\begin{cases} E = 0 \quad \text{on } \Gamma \\ \displaystyle\int_\Omega \left\{ \frac{1}{\mu} \left[\frac{\partial E}{\partial z} \frac{\partial v}{\partial z} + \frac{1}{r^2} \left(E + r \frac{\partial E}{\partial r} \right) \left(v + r \frac{\partial v}{\partial r} \right) \right] - (\omega^2 \epsilon - \jmath \omega \sigma) E v \right\} r \, \mathrm{d}r \, \mathrm{d}z \, . \\ \quad = \jmath \omega \int_{\partial D} r \boldsymbol{J}_s^{\text{imp}} \cdot \boldsymbol{v} \, \mathrm{d}s, \quad \text{for every test function } v, v = 0 \quad \text{on } \Gamma \end{cases} \tag{2.4}$$

(Here $\mathrm{d}s^2 = \mathrm{d}r^2 + \mathrm{d}z^2$).

Notice that the original Neumann boundary condition on Γ translates now into a Cauchy (Robin) boundary condition,

$$\frac{\partial E}{\partial r} + \frac{n_r}{n} E = \jmath \omega \boldsymbol{J}_s^{\text{imp}}, \tag{2.5}$$

where $\boldsymbol{n} = (n_r, n_z)^{\mathrm{T}}$.

The solution is required with great accuracy at the receiving antenna where the field is several orders of magnitude weaker compared to the emitter. It turns out that this represents an essential difficulty to all existing *h*- and *hp*-adaptive strategies. We will return to this problem in Section 4, with a suitable goal-oriented *hp*-adaptive finite element method in hand. Before we present the scheme, let us briefly review the basic principles of both goal-oriented and *hp*-adaptivity.

2.2. Basic principles of goal-oriented adaptivity

During the last decade, goal-oriented adaptivity for PDEs has been a topic of permanent scientific and engineering interest, and several basic methodologies have been proposed (see e.g., [2–5,13,14,17]). In

comparison with the adaptivity in energy norm which attempts to minimize the energy of the residual of the approximate solution, the goal-oriented approach attempts to control concrete features of the solved problem (*quantities of interest*). Goal-oriented adaptive techniques are designed to achieve precise resolution in quantities of interest with significantly less degrees of freedom than the standard adaptive schemes.

2.2.1. Quantities of interest

Very often quantities of interest can be represented as bounded linear functionals of the solution. For example, the goal in the motivating problem from the previous section leads to a functional of the type

$$L(\boldsymbol{u}) = \int_{\Omega_s} \boldsymbol{u}(x)\,\mathrm{d}x, \tag{2.6}$$

(to be shown in more detail in Section 4.1) where Ω_s is a subdomain of the computational domain Ω. However, there are numerous quantities of interest which cannot be directly expressed in terms of bounded linear functionals. A particularly important example is the value of the solution $\boldsymbol{u}$ at a selected point x_0 in domain Ω. In such cases we may try to find a suitable approximation of the quantity of interest, e.g.,

$$L(\boldsymbol{u}) = \frac{1}{|B(x_0, r)|} \int_{B(x_0,r)} \boldsymbol{u}(x)\,\mathrm{d}x, \tag{2.7}$$

where $B(x_0, r) \subset \Omega$ is a ball with the center x_0 and a sufficiently small radius r. Another possible approach to pointwise values is the use of *regularizing mollifiers* (see e.g. [12]).

2.2.2. Overview of ideas leading to the formulation of the dual problem

- Consider a problem to find a solution $\boldsymbol{u}$ lying in a Hilbert space V and satisfying the weak formulation
  $$b(\boldsymbol{u}, \boldsymbol{v}) = f(\boldsymbol{v}) \tag{2.8}$$
  for all $\boldsymbol{v} \in V$, b being an elliptic bilinear form defined on $V \times V$ and $f \in V'$.
- Consider the discrete problem
  $$b(\boldsymbol{u}_{h,p}, \boldsymbol{v}_{h,p}) = f(\boldsymbol{v}_{h,p}) \tag{2.9}$$
  for all $\boldsymbol{v}_{h,p} \in V_{h,p}$ where $V_{h,p} \subset V$ is a polynomial finite element approximation of space V.
- Define the error $\boldsymbol{e}_{h,p} = \boldsymbol{u} - \boldsymbol{u}_{h,p}$ and consider the residual
  $$\boldsymbol{r}_{h,p}(\boldsymbol{v}_{h,p}) = f(\boldsymbol{v}_{h,p}) - b(\boldsymbol{u}_{h,p}, \boldsymbol{v}_{h,p}). \tag{2.10}$$
- Relate the residual $\boldsymbol{r}_{h,p}$ to the error in the quantity of interest, i.e. find $G \in V''$ such that
  $$G(\boldsymbol{r}_{h,p}) = L(\boldsymbol{e}_{h,p}).$$
- By reflexivity, G can be related to an element $\boldsymbol{v}$ in the original space (*influence function*),
  $$G(\boldsymbol{r}_{h,p}) = \boldsymbol{r}_{h,p}(\boldsymbol{v}) = f(\boldsymbol{v}) - b(\boldsymbol{u}_{h,p}, \boldsymbol{v}) = b(\boldsymbol{u}, \boldsymbol{v}) - b(\boldsymbol{u}_{h,p}, \boldsymbol{v}) = \underbrace{b(\boldsymbol{e}_{h,p}, \boldsymbol{v}) = L(\boldsymbol{e}_{h,p})}, \tag{2.11}$$
  where $\boldsymbol{v}$ is the solution to the *dual problem:*
- Find $\boldsymbol{v} \in V$ such that
  $$b(\boldsymbol{u}, \boldsymbol{v}) = L(\boldsymbol{u}) \tag{2.12}$$
  for all $\boldsymbol{u} \in V$.
- Consider the discrete dual problem
  $$b(\boldsymbol{u}, \boldsymbol{v}_{h,p}) = L(\boldsymbol{u}) \tag{2.13}$$
  for all it $\boldsymbol{u} \in V_{h,p}$.

- Estimate the error in the quantity of interest by means of the errors *in energy norms* for both the primal and dual problem:

$$|L(\boldsymbol{u}) - L(\boldsymbol{u}_{h,p})| = |L(\boldsymbol{u} - \boldsymbol{u}_{h,p})| = |b(\boldsymbol{u} - \boldsymbol{u}_{h,p}, \boldsymbol{v})| = |b(\boldsymbol{u} - \boldsymbol{u}_{h,p}, \boldsymbol{v} - \boldsymbol{v}_{h,p})| \leqslant C \sum_{K \in \tau_{h,p}} \|\boldsymbol{u} - \boldsymbol{u}_{h,p}\|_{e,K} \|\boldsymbol{v} - \boldsymbol{v}_{h,p}\|_{e,K}. \tag{2.14}$$

(Standard orthogonality property for the error in the solution was used.)

2.3. Brief review of hp-adaptivity

The *hp*-version of the finite element method combines the adaptivity in h (spatial refinements) with the adaptivity in p (variation of the degree of polynomial approximation in finite elements) in a unique way. The basic advantage with respect to other h- or p- only adaptive schemes is that the method achieves an exponential convergence in the energy norm for linear elliptic boundary value problems with possibly singular solutions. In other words, as opposed to h- and p-methods, the simultaneous refinements in both h and p allow to concentrate the degrees of freedom at singularities in a way which is sufficient to control them numerically. Such singularities are natural for domains with reentrant corners, for points on the boundary where the boundary conditions change their type, and intersections of material interfaces. Their efficient resolution is crucial in many practical problems arizing in the engineering practice.

Nowadays, the theory of the *hp*-version of the finite element method is well-established and founded on solid results mostly due to the efforts of Babuška and coworkers. However, the practical realization of fully automatic and robust 3D *hp*-adaptive algorithms still presents many serious difficulties mainly due to excessive programming complexity. We refer to [6,8,15] and references therein.

2.4. Mesh optimization procedure for energy-driven hp-adaptivity

An adaptive finite element strategy is usually based on some information about the local approximation error that decides where the finite element mesh is to be refined. Most approaches are based on the evaluation of error estimators of various kinds on each mesh element. This seems to be sufficient for schemes which are adaptive either in h or in p only, because it is only the magnitude of the error in an element which decides about the refinement of the element. However, the *hp*-adaptivity brings more choices for an element to be refined: there is the possibility to perform either a p-refinement only, or to split the element spatially with various distributions of the polynomial degree p for its sons. Obviously, we must be critical when deciding between various refinement possibilities, which means that we must take into account both the invested number of degrees of freedom and the profit which the various refinement options bring. Such refinement options for a mesh element are called *competitive element refinements*.

An original approach based on the maximization of the decrease rate for the local *hp*-interpolation error with respect to a *reference solution* was presented in [15], A reference solution $\boldsymbol{u}_{\text{ref}}$ is an approximation of the exact solution u which is closer to the exact solution than the original approximation $\boldsymbol{u}_{h,p}$.

Hence, the difference $\boldsymbol{u}_{\text{ref}} - \boldsymbol{u}_{h,p}$ is capable of delivering useful information not only about the magnitude but also about the concrete *shape* of the error $\boldsymbol{e}_{h,p}$. The reference function can be obtained in several different ways (see e.g., [15] where for this purpose Babuška's *extraction formulas* were used).

2.4.1. Reference solutions on globally refined grids

In [8], reference solutions are computed as approximate solutions corresponding to *hp*-grids obtained by a uniform h- and p-refinement such that $h \to h/2$ and $p \to p + 1$ for all mesh elements. By $\boldsymbol{u}_{h/2,p+1}$ we denote

the fine grid solution. The reader may object that the computation of $\boldsymbol{u}_{h/2,p+1}$ becomes prohibitive in 3D. However, one must not forget that *hp*-adaptivity is designed to reduce the number of degrees of freedom in 3D by orders of magnitude with respect to, e.g., standard *h*-adaptive schemes. Numerical experience shows that this is a realistic expectation, which we hope to confirm by large 3D computations in the near future.

Let us remark that for *h*-adaptivity the *hp*-strategy reduces $\boldsymbol{u}_{h/2,p+1}$ to $\boldsymbol{u}_{h/2}$ (i.e. the reference solution is constructed by uniform *h*-refinement only). This is sufficient as. in this case, the variation in p is not involved in the mesh optimization process.

2.4.2. Error as the difference between the reference solution and its interpolant

It is our aim to minimize the error in energy norm

$$\|\boldsymbol{e}\|_e^2 = \|\boldsymbol{u} - \boldsymbol{u}_{h,p}\|_e^2. \tag{2.15}$$

In the language of element contributions we can write

$$\|\boldsymbol{u} - \boldsymbol{u}_{h,p}\|_e^2 = \sum_{K \in \tau_{h,p}} \|\boldsymbol{u} - \boldsymbol{u}_{h,p}\|_{e,K}^2, \tag{2.16}$$

where $\tau_{h,p}$ stands for the *hp*-mesh and K for a mesh element. Obviously the minimization of $\|\boldsymbol{u} - \boldsymbol{u}_{h,p}\|_{e,K}^2$ cannot be done locally. But, asymptotically, we can achieve the same goal by minimizing

$$\|\boldsymbol{u}_{\text{ref}} - \Pi_{h,p}\boldsymbol{u}_{\text{ref}}\|_{e,K}^2 \tag{2.17}$$

on all $K \in \tau_{h,p}$ where $\Pi_{h,p}$ is a suitable *projection-based interpolation.*

Let us emphasize that the replacement of $\boldsymbol{u}_{h,p}$ with $\Pi_{h,p}\boldsymbol{u}_{\text{ref}}$ is essential for the adaptive strategy, since it opens the possibility for minimization of the approximate error bound (2.17) by suitable adjustments of the *hp*-mesh *locally*, one element at a time. The same approach will be used later in the goal-oriented case, in the estimate (3.22).

2.4.3. Projection-based interpolation

Finite element interpolants can be constructed very easily for nodal elements whose degrees of freedom are typically defined on large sets of functions (i.e. both inside and outside the local finite element polynomial space). The situation is completely different for elements whose degrees of freedom are defined via hierarchic shape functions, since they are defined in the local finite element space only. Hence, for hierarchic elements, the interpolation must be combined with suitable *projection* onto the finite element space. The definition of suitable projection-based interpolation operators is not trivial (see e.g., [7]). The operators must satisfy the following conditions:

- The interpolant must lie in the finite element space.
- The interpolation must be *local*, i.e. it must be capable of projecting a function onto an element using information accessible from inside of the element only.
- The interpolation must be *optimal*, i.e. deliver the same convergence rates as the global approximation.

The projection-based interpolation $\Pi_{h,p}$ (of reference solution $\boldsymbol{u}_{\text{ref}}$), analyzed in [7], consists of three steps:

- Evaluation of $\boldsymbol{u}_{\text{ref}}$ at mesh vertices and its extension to the element interior—resulting in (bi)linear vertex interpolant denoted by $\boldsymbol{u}_1$.
- Projection of $\boldsymbol{u}_{\text{ref}} - \boldsymbol{u}_1$ in H_0^1 on edges and its extension to the element interior—resulting in edge interpolant denoted by $\boldsymbol{u}_2$: this step involves a discrete minimization problem (= solution of a system of linear equations) on each edge.

- Projection of $\boldsymbol{u}_{\text{ref}} - \boldsymbol{u}_1 - \boldsymbol{u}_2$ on the element bubble functions; this step involves one solution of a system of linear equations for each element.

With a suitable projection-based interpolation in hand, one step of the mesh optimization looks as follows (we refer to [8] for the full description of the algorithm):

(1) Perform the global *hp*-refinement and compute fine mesh solution $\boldsymbol{u}_{h/2,p+1}$.
(2) Compute elementwise error $\|\boldsymbol{u}_{h/2,p+1} - \boldsymbol{u}_{h,p}\|^2_{e,K}$ for all $T \in \tau_{h,p}$.
(3) Determine the element isotropy flags (= determine if the element is going to be refined isotropically or anisotropically).
(4) Determine optimal refinement for each edge in the mesh $\tau_{h,p}$ using competitive refinements.
(5) Determine the maximum edge error decrease rate and identify all edges with error decrease equal at least to (e.g.) one third of the maximal one; those edges are going to be refined. Let us remark that this concrete choice is based on our numerical experience—the algorithm will work with 1/4, 1/2 and other values as well. It is extremely difficult to investigate the optimality of this value rigorously.
(6) Use the information about edge *h*-refinements and the element isotropy flags to decide about *h*-refinements for all elements. After this step, the topology of the new mesh is determined.
(7) Determine optimal orders of approximation for all element interiors monitoring the error decrease rate.
(8) Enforce the *minimum rule* to all edges in the mesh: order of approximation for an edge must be equal to the minimum of orders for the adjacent elements.

The *hp*-adaptive strategy starts with an initial mesh and repeats the mesh-optimization procedure until a sufficient accuracy of the solution (measured in the energy norm of the difference of $\boldsymbol{u}_{h/2,p+1} - \boldsymbol{u}_{h,p}$) is reached. The reader may notice that the stopping criterion is the only reason for the computation of the approximation $\boldsymbol{u}_{h,p}$ on the coarse grid—$\boldsymbol{u}_{h,p}$ is *not used for the mesh optimization*. The solution $\boldsymbol{u}_{h/2,p+1}$ can be used as a final result.

Let us emphasize that strategies based on reference solutions are not the only option—for example, we refer to [1] for an alternative strategy based on monitoring local *h*-convergence rates.

3. Fully automatic adaptive strategies

Now we have given enough background to introduce the goal-oriented *hp*-adaptive strategy, which is a general representant of a whole class of goal-oriented and energy-driven *h*-, *p*- and *hp*-adaptive schemes. Notice that goal-oriented adaptivity reduces to energy-driven when the dual problem is identical to the primal one (which, obviously, needs not be solved twice). The *hp*-adaptivity can be reduced to *h*- and *p*-adaptivity by fixing either *p* or *h*, respectively. Later in this section we will mention these simplifications for comparison purposes.

3.1. Goal-oriented hp-adaptivity

Let us start with the most general case of goal-oriented *hp*-adaptivity. The basic difference between the original energy driven *hp* adaptive strategy from [8], and the goal-oriented approach, is that instead of minimizing the error in the energy norm (2.15), we will minimize the error in the quantity of interest,

$$\|L(\boldsymbol{u}_{h/2,p+1}) - L(\boldsymbol{u}_{h,p})\|. \tag{3.18}$$

Here $\boldsymbol{u}_{h/2,p+1}$ stands for the fine mesh solution corresponding to the globally refined mesh $\tau_{h/2,p+1}$. Replacing the exact solution $\boldsymbol{u}$ and the (exact) dual solution $\boldsymbol{v}$ with the corresponding fine mesh solutions $\boldsymbol{u}_{h/2,p+1}$, $\boldsymbol{v}_{h/2,p+1}$, respectively, we repeat now the steps discussed in Section 2.2 to arrive at the following identity,

$$|L(\boldsymbol{u}_{h/2,p+1}) - L(\boldsymbol{u}_{h,p})| = b(\boldsymbol{u}_{h/2,p+1} - \boldsymbol{u}_{h,p}, \boldsymbol{v}_{h/2,p+1} - \boldsymbol{v}_{h,p}). \tag{3.19}$$

We assume that the bilinear form $b(\boldsymbol{u}, \boldsymbol{v})$ can be split into a bilinear, positive definite part $a(\boldsymbol{u}, \boldsymbol{v})$ and a compact perturbation $c(\boldsymbol{u}, \boldsymbol{v})$, see [9],

$$b(\boldsymbol{u}, \boldsymbol{v}) = a(\boldsymbol{u}, \boldsymbol{v}) + c(\boldsymbol{u}, \boldsymbol{v}). \tag{3.20}$$

Recall that in (3.19) $\boldsymbol{u}_{h/2,p+1}$ and $\boldsymbol{u}_{h,p}$ are fine and coarse grid solution to the original problem, $\boldsymbol{v}_{h/2,p+1}$ is the fine grid solution of the dual problem. and $\boldsymbol{v}_{h,p}$ stands for any coarse grid test function. We make now the following assumptions.

(1) We select for $\boldsymbol{v}_{h,p}$the projection-based interpolant of fine mesh dual problem solution,

$$\begin{aligned} L(\boldsymbol{u}_{h/2,p+1}) - L(\boldsymbol{u}_{h,p}) = {} & b(\boldsymbol{u}_{h/2,p+1} - \Pi\boldsymbol{u}_{h/2,p+1}, \boldsymbol{v}_{h/2,p+1} - \Pi\boldsymbol{v}_{h/2,p+1}) \\ & b(\Pi\boldsymbol{u}_{h/2,p+1} - \boldsymbol{u}_{h,p}, \boldsymbol{v}_{h/2,p+1} - \Pi\boldsymbol{v}_{h/2,p+1}). \end{aligned} \tag{3.21}$$

(2) We neglect the second term corresponding to the contribution of the difference between the coarse grid interpolant $\Pi\boldsymbol{u}_{h/2,p+1}$ and coarse grid solution.
This leads to the estimate

$$\begin{aligned} & |L(\boldsymbol{u}_{h/2,p+1}) - L(\boldsymbol{u}_{h,p})| \\ & \quad \leqslant \sum_{K\in\tau_{h,p}} |b_K(\boldsymbol{u}_{h/2,p+1} - \Pi\boldsymbol{u}_{h/2,p+1}, \boldsymbol{v}_{h/2,p+1} - \Pi\boldsymbol{v}_{h/2,p+1})| \\ & \quad \leqslant \sum_{K} \left\{ |a_K(\boldsymbol{u}_{h/2,p+1} - \Pi\boldsymbol{u}_{h/2,p+1}, \boldsymbol{v}_{h/2,p+1} - \Pi\boldsymbol{v}_{h/2,p+1})| + |c_K(\boldsymbol{u}_{h/2,p+1} - \Pi\boldsymbol{u}_{h/2,p+1}, \boldsymbol{v}_{h/2,p+1} - \Pi\boldsymbol{v}_{h/2,p+1})| \right\} \\ & \quad \leqslant \sum_{K} (1 + M_K) \|\boldsymbol{u}_{h/2,p+1} - \Pi\boldsymbol{u}_{h/2,p+1}\|_{e,K} \|\boldsymbol{v}_{h/2,p+1} - \Pi\boldsymbol{v}_{h/2,p+1}\|_{e,K}. \end{aligned} \tag{3.22}$$

Here b_K, a_K, c_K denote element contributions to global forms b, a, c respectively and M_K stands for the continuity constant of bilinear form c_K,

$$|c_K(\boldsymbol{u}_{h/2,p+1} - \Pi\boldsymbol{u}_{h/2,p+1}, \boldsymbol{v}_{h/2p+1} - \Pi\boldsymbol{v}_{h/2,p+1})| \leqslant M_K \|\boldsymbol{u}_{h/2,p+1} - \Pi\boldsymbol{u}_{h/2,p+1}\|_{e,K} \|\boldsymbol{v}_{h/2,p+1} - \Pi\boldsymbol{v}_{h/2,p+1}\|_{e,K}. \tag{3.23}$$

(3) Since the constant M_K corresponds to a compact perturbation of an elliptic operator, we expect it to be asymptotically (both in h and p) converging to zero, and we shall neglect it in our estimate.
This leads to the final estimate,

$$|L(\boldsymbol{u}_{h/2,p+1}) - L(\boldsymbol{u}_{h,p})| \leqslant \sum_{K\in\tau_{h,p}} \|\boldsymbol{u}_{\text{ref}} - \Pi_{h,p}\boldsymbol{u}_{\text{ref}}\|_{e,K} \|\boldsymbol{v}_{\text{ref}} - \Pi_{h,p}\boldsymbol{v}_{\text{ref}}\|_{e,K}, \tag{3.24}$$

which is approximate in sense of neglecting the difference between fine mesh solution and fine mesh solution interpolant in (1). Consequently, instead of minimizing the projection based interpolation error,

$$\|\boldsymbol{u}_{h/2,p+1} - \Pi_{h,p}\boldsymbol{u}_{h/2,p+1}\|^2 = \sum_{K} \|\boldsymbol{u}_{h/2,p+1} - \Pi_{h,p}\boldsymbol{u}_{h/2,p+1}\|^2_{e,K}, \tag{3.25}$$

we shall modify the original *hp* strategy to minimize now estimate (3.24). The steps of the algorithm are analogous to those discussed in Section 2.4.

(1) Compute element contributions to estimate (3.24),

$$\|\boldsymbol{u}_{h/2,p+1} - \Pi_{h,p}\boldsymbol{u}_{h/2,p+1}\|_{e,K}\|\boldsymbol{v}_{h/2,p+1} - \Pi_{h,p}\boldsymbol{v}_{h/2,p+1}\|_{e,K}, \tag{3.26}$$

for all $T \in \tau_{h,p}$.

(2) Determine the element isotropy flags. An element is declared to be a candidate for an anisotropic refinement if *both* differences $\boldsymbol{u}_{h/2,p+1} - \boldsymbol{u}_{h,p}$ and $\boldsymbol{v}_{h/2,p+1} - \boldsymbol{v}_{h,p}$ represent the same anisotropic behavior.

(3) Determine optimal refinement for each edge e in the current mesh $\tau_{h,p}$ comparing competitive refinements. Use product of the interpolation errors for the primal and dual problems in place of the interpolation error of the fine mesh solution,

$$\|\boldsymbol{u}_{h/2,p+1} - \Pi_{h,p}\boldsymbol{u}_{h/2,p+1}\|_{H^{\frac{1}{2}}_{00}(e)}\|\boldsymbol{v}_{h/2,p+1} - \Pi_{h,p}\boldsymbol{v}_{h/2,p+1}\|_{H^{\frac{1}{2}}_{00}(e)}. \tag{3.27}$$

The $H^{\frac{1}{2}}_{00}(e)$-norm on the edge e is defined in a standard way as the H^1-seminorm of a harmonic extension into element interior (see e.g., [7]).

(4) Determine the maximum edge error decrease rate and identify all edges with error decrease greater or equal than one third of the maximal one; those edges are going to be refined.

(5) Use the information about edge h-refinements and the element isotropy flags to decide about h-refinements for all elements.

(6) Determine optimal orders of approximation for all element interiors monitoring the decrease rate of the product of the element interpolation errors (3.26).

(7) Enforce the *minimum rule* for all edges in the mesh: order of approximation for an edge must be equal to the minimum of orders for the adjacent elements.

With the one step minimization strategy described above, the ultimate goal-oriented *hp* strategy looks as follows.

(1) Initiate $k := 0$.
(2) Consider mesh $\tau^k_{h,p}$ and corresponding space of functions $V^k_{h,p}$.
(3) Solve primal problem on the coarse mesh: $b(\boldsymbol{u}^k_{h,p}, \boldsymbol{v}) = f(\boldsymbol{v})$, for all $\boldsymbol{v} \in V^k_{h,p}$.
(4) Solve dual problem on the coarse mesh: $b(\boldsymbol{u}, \boldsymbol{v}^k_{h,p}) = L(\boldsymbol{u})$, for all $\boldsymbol{u} \in V^k_{h,p}$.
(5) Construct globally *hp*-refined mesh $\tau^k_{h/2,p+1}$ and the corresponding finite element space $V^k_{h/2,p+1}$.
(6) Solve primal problem on the fine mesh: $b(\boldsymbol{u}^k_{h/2,p+1}, \boldsymbol{v}) = f(\boldsymbol{v})$, for all $\boldsymbol{v} \in V^k_{h/2,p+1}$.
(7) Solve dual problem on the fine mesh: $b(\boldsymbol{u}, \boldsymbol{v}^k_{h/2,p+1}) = L(\boldsymbol{u})$, for all $\boldsymbol{u} \in V^k_{h/2,p+1}$.
(8) Compute estimate (3.24). If the estimated difference (relative to fine mesh goal $L(\boldsymbol{u}_{h/2,p+1})$) is within the prescribed tolerance, quit.
(9) Apply the mesh optimization procedure described above to construct next optimal mesh $\tau^{k+1}_{h,p}$.

Remark

(1) Similarly as in [8], we replace the $H^{\frac{1}{2}}_{00}(e)$ norm with a weighted $H^1_0(e)$ norm, see [8] for details.
(2) Notice that the stopping criterion is based on the actual difference of the fine and coarse mesh goals and not its estimate.

3.2. Energy driven h-adaptive algorithm

One of the goals of the presented work is to gain some experience with how much we can gain using *hp*-adaptivity when compared with *h*-adaptivity based on quadratic elements. The choice of quadratic elements

seems to be fair as, in general, they deliver vastly superior results to linear elements, and their implementation is much simpler than, say, cubic elements. Quadratic element, for instance, have only one d.o.f. (scalar case) per edge, face, and element interior (no orientation needed !) and present a good balance between accuracy and complexity of the corresponding implementation.

First let us discuss a simplification of the goal-oriented *hp*-adaptive procedure from the previous section leading to energy-driven *h*-adaptivity. Given a coarse mesh τ_h^k and corresponding finite element space V_h^k, we construct the next coarse mesh τ_h^{k+1} as follows:

(1) Solve primal problem on the coarse mesh: $b(\boldsymbol{u}_h^k, \boldsymbol{v}) = f(\boldsymbol{v})$ for all $\boldsymbol{v} \in V_h^k$.
(2) Construct globally *h*-refined mesh $\tau_{h/2}^k$ and the corresponding FE space $V_{h/2}^k$.
(3) Solve primal problem on the fine mesh: $b(\boldsymbol{u}_{h/2}^k, \boldsymbol{v}) = f(\boldsymbol{v})$, for all $\boldsymbol{v} \in V_{h/2}^k$.
(4) Compute the difference between the coarse and fine mesh solutions,

$$\|\boldsymbol{u}_{h/2}^k - \boldsymbol{u}_h^k\|_e^2 = \sum_{K \in \tau_h^k} \|\boldsymbol{u}_{h/2}^k - \boldsymbol{u}_h^k\|_{e,K}^2.$$

When computing the element contributions, determine the anisotropy flags for the elements.
(5) Quit if the error estimate is below the prescribed tolerance.
(6) Determine the maximum element contribution to the error estimate, and refine all elements that contribute with error within one third of the maximum one. Use the isotropy flags to decide between the isotropic and anisotropic refinements.

3.3. Goal-driven h-adaptive algorithm

Given a coarse mesh τ_h^k and corresponding finite element space V_h^k, we construct the next coarse mesh τ_h^{k+1} as follows:

(1) Solve primal problem on the coarse mesh: $b(\boldsymbol{u}_h^k, \boldsymbol{v}) = f(\boldsymbol{v})$, for all $\boldsymbol{v} \in V_h^k$.
(2) Solve dual problem on the coarse mesh: $b(\boldsymbol{u}, \boldsymbol{v}_h^k) = L(\boldsymbol{u})$, for all $\boldsymbol{u} \in V_h^k$.
(3) Construct globally *h*-refined mesh $\tau_{h/2}^k$ and the corresponding FE space $V_{h/2}^k$.
(4) Solve primal problem on the fine mesh: $b(\boldsymbol{u}_{h/2}^k, \boldsymbol{v}) = f(\boldsymbol{v})$, for all $\boldsymbol{v} \in V_{h/2}^k$.
(5) Solve dual problem on the fine mesh: $b(\boldsymbol{u}, \boldsymbol{v}_{h/2}^k) = L(\boldsymbol{u})$, for all $\boldsymbol{u} \in V_{h/2}^k$.
(6) Compute the estimate of the difference in goal for the coarse and fine mesh solutions,

$$|L(\boldsymbol{u}_{h/2}^k) - L(\boldsymbol{u}_h^k)| \lesssim \sum_{K \in \tau_h^k} \|\boldsymbol{u}_{h/2}^k - \boldsymbol{u}_h^k\|_{e,K} \|\boldsymbol{v}_{h/2}^k - \boldsymbol{v}_h^k\|_{e,K}.$$

When computing the element contributions, determine the anisotropy flags for the elements.
(7) Quit if the difference in goals for the fine and coarse mesh solutions is below the prescribed tolerance.
(8) Determine the maximum element contribution to the error estimate, and refine all elements that contribute with error within one third of the maximum one. Use the isotropy flags to decide between the isotropic and anisotropic refinements.

3.4. Numerical illustration: Laplace equation

We consider the standard L-shape Ω domain problem, see [8].
We solve the Laplace equation

$$-\Delta u = 0 \tag{3.28}$$

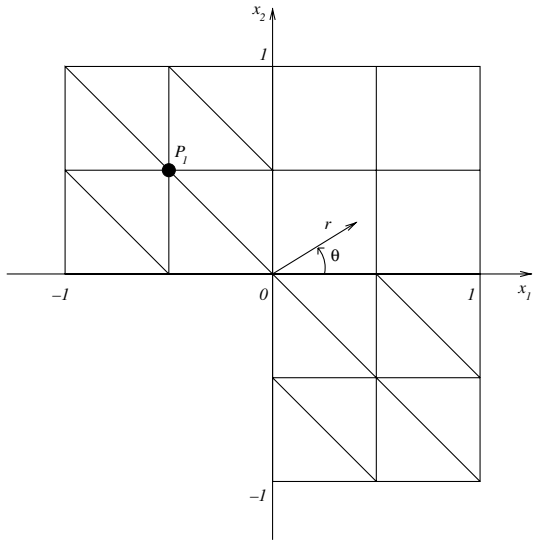

Fig. 2. Geometry and initial mesh.

in Ω, with Dirichlet boundary conditions $u(x) = \varphi(x)$ for all $x \in \partial\Omega$. Function φ is chosen to be compatible with the harmonic function

$$u(x_1, x_2) = r^{2/3} \sin(2\theta/3 + \pi/3), \tag{3.29}$$

where (r, θ) are standard polar coordinates. Derivatives of the solution are singular at origin $(0, 0)$ (Fig. 2).

The goal of our computation is the average value of the solution u over a small neighborhood Ω_s of point $P_1 = (-0.5, 0.5)$, defined as follows: consider the mesh edges $e_j, j = 1, 2, \ldots, 6$, starting at P_1. On each of them construct a point Q_j whose distance from P_1 is

$$|Q_j - P_1| = \frac{|e_j|}{2^{N_s}}, \tag{3.30}$$

$N_s = 5$. The neighborhood Ω_s is defined as the convex envelope of points $Q_1, Q_2, \ldots, Q_6$, as illustrated in Fig. 3.

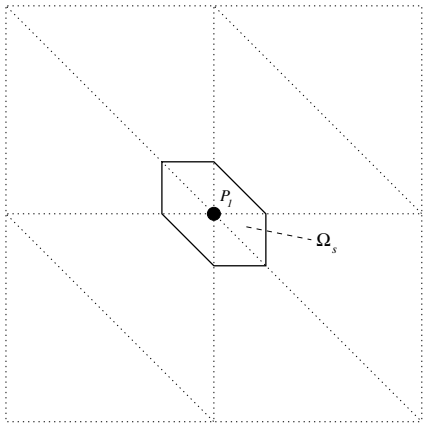

Fig. 3. The neighborhood Ω_s of the point P_1 (the illustration roughly corresponds to $N_s = 2$).

Let us mention that this concrete choice of Ω_s has been motivated by the ease of computer implementation of the numerical quadrature over Ω_s only, and that Ω_s does not change during the adaptive procedure.

Figs. 4–7 show meshes which have been obtained to yield a relative error in the quantity of interest to be less than 10^{-5}. Scale on the right hand side indicates the order of polynomial approximation, starting with $p = 1$.

Fig. 8 shows the history of the relative error in goal for all four tested approaches. The x-axis represents the number of degrees of freedom.

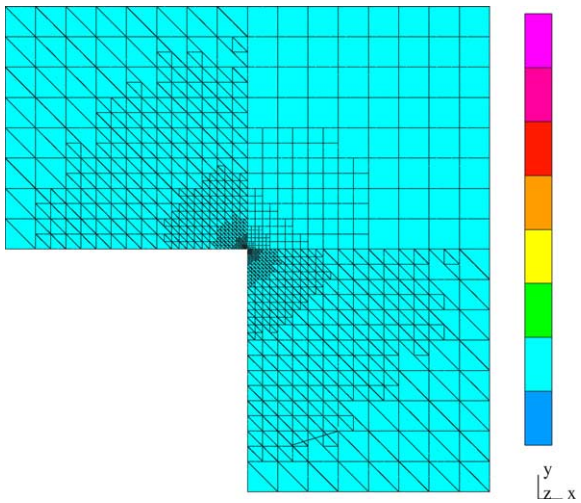

Fig. 4. Energy-based h-adaptivity. Mesh after 18 h-refinements (all elements are second-order), number of DOF = 3114.

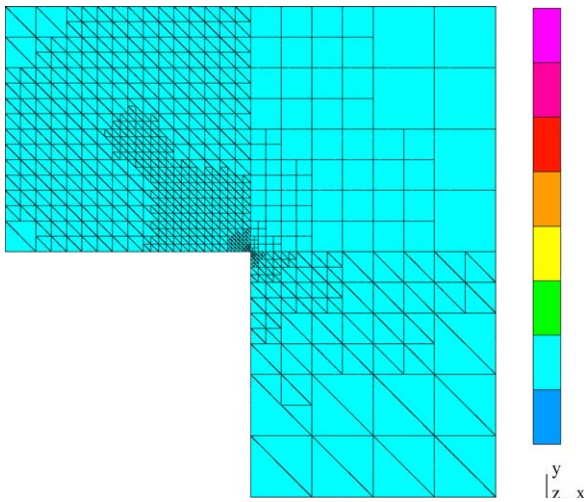

Fig. 5. Goal-oriented h-adaptivity. Mesh after 17 h-refinements (all elements are second-order), number of DOF = 2448.

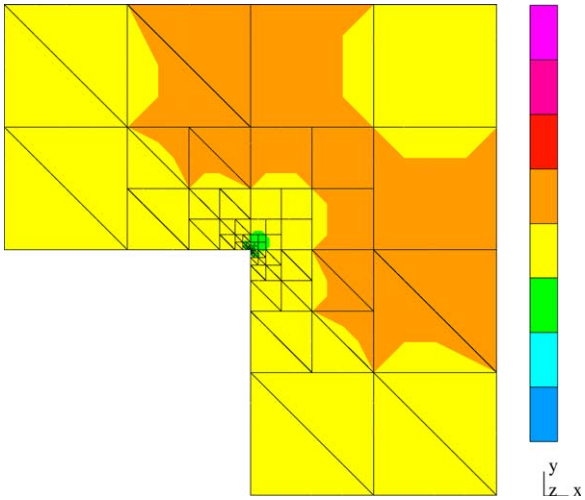

Fig. 6. Energy-based *hp*-adaptivity. Mesh after 15 *hp*-refinements, number of DOF = 1366.

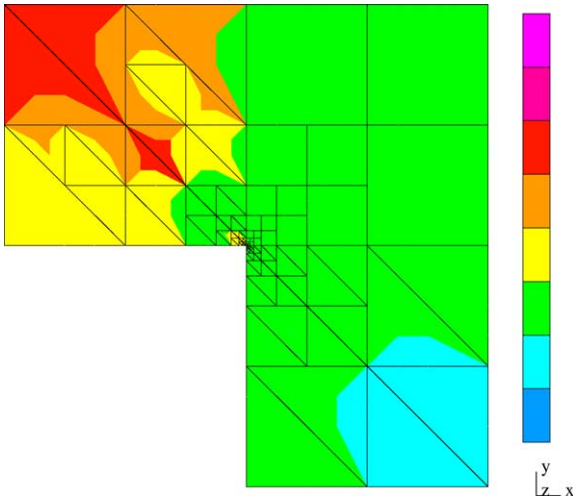

Fig. 7. Goal-oriented *hp*-adaptivity. Mesh after 10 *hp*-refinements, number of DOF = 803.

4. Application to the radiation problem

Finally we return to the motivating problem introduced in Section 2.1.

4.1. Numerical setting

We shall describe now the geometry of the domain, initial mesh and the quantity of interest in more detail. All values below are given in meters (some of them being converted from inches).

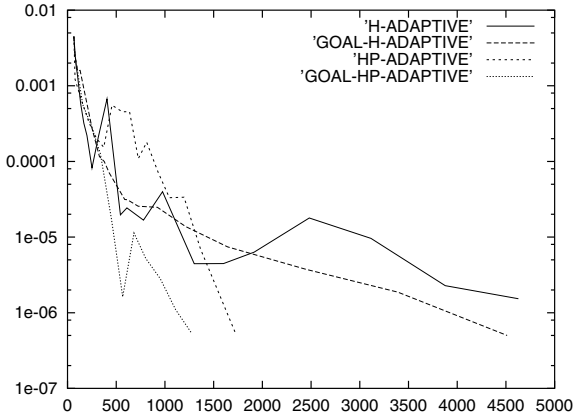

Fig. 8. Relative error wrt. the exact solution in goal.

4.1.1. Geometry of domain and initial mesh

Besides the emitting antenna, a receiving antenna, occupying another subdomain $D_1 \subset \Omega$ is placed into the computational domain. Both antennas have identical form of a single axisymmetric ring of radius $r_a = 0.03048$. The cross-section of the antennas is circular with radius $r_c = 0.000718$. Midpoints of the emitting and receiving antenna in the axisymmetric geometry are $P_0 = (0.03048, 0)$ and $P_1 = (0.03048, 0.5)$, respectively. The computational domain with the initial mesh is shown in Fig. 9.

Grid points in the r- and z-direction are listed in Tables 1 and 2, respectively.

We have to impose certain geometrical gradation of the mesh towards the antennas in order to minimize the initial mesh error, but notice that both very large and very long thin elements are left in the mesh. Certain optimization of the initial mesh is required since it significantly influences the convergence of the adaptive scheme. However, it is our aim to reduce the work related to the generation of initial meshes as much as possible.

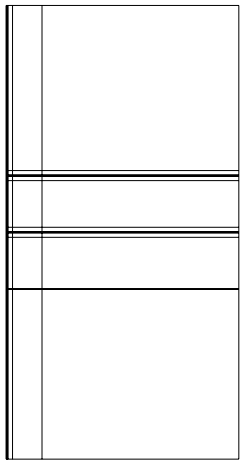

Fig. 9. Geometry and initial mesh on Ω.

Table 1
Grid points in the r-direction

0.02	0.0254	0.029214	0.030226	0.030734
0.031746	0.03738	0.075042	0.326024	2.0

Table 2
Grid points in the z-direction

−2.0	−0.500254	−0.499746	−0.044248	−0.007003
−0.001266	−0.000254	0.000254	0.001266	0.007003
0.044248	0.455752	0.492997	0.498734	0.499746
0.500254	0.501266	0.507003	0.544248	2.0

Curvilinear elements are used to model both antennas as true circles. This turned out to be necessary in order to avoid non-physical singularities and the use of too many degrees of freedom necessary to resolve them.

Recall that we model the emitting antenna by means of a Cauchy boundary condition for E in order to avoid refinements in its interior. Hence, our computational domain Ω is obtained after subtracting the emitting antenna (i.e. circle with midpoint P_0 and radius r_c) from the rectangle $[0.02, 2.0] \times [-2.0, 2.0]$. The subdomain $\Omega_m \subset \Omega$, $\Omega_m = [0.02, 0.0254] \times [-2.0, 2.0]$ represents a metallic mandrel with the material properties $\mu = 1$, $\sigma = 10^7$, $\epsilon = 1$. The same material properties are chosen also for the receiving antenna.

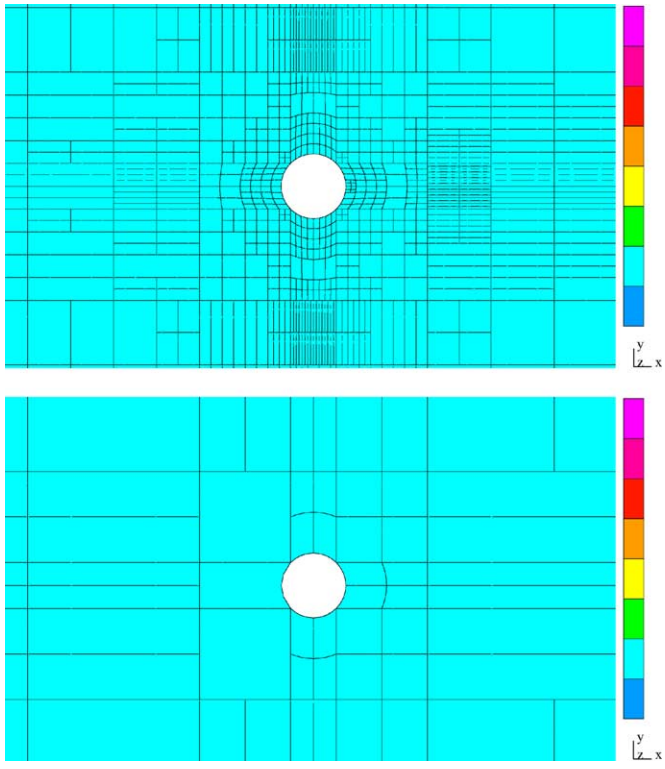

Fig. 10. Energy-based h-adaptivity (above) and goal-oriented h-adaptivity (below), zoom = 1000 towards the emitting antenna.

The rest of Ω represents mud and soil with the material properties $\mu = 1$, $\sigma = 1$, $\epsilon = 1$. Here μ stands for the permeability, σ for the electrical conductivity and ϵ for the dielectric constant.

The frequency and angular frequency of the harmonic field have the values $f = 2 \times 10^6$, $\omega = 2\pi f$.

4.1.2. Goal of computation

Our objective here is to predict the value of

$$N(E) = 20 \log_{10} \int_{D_1} Er \, dr \, dz, \tag{4.31}$$

representing a measure of the electromagnetic force at the receiving antenna in decibels (dB). Hence the goal is to find an approximation $E_{h,p}$ of E such that

$$|N(E_{h,p}) - N(E)| \leqslant TOL, \tag{4.32}$$

where E is the (unknown) exact solution. We look for a suitable linear functional of interest for the dual problem approximating $N(E)$. Assuming that the value

$$\int_{B(P_1, r_c)} E_{h,p} r \, dr \, dz, \tag{4.33}$$

corresponding to the approximate solution will be close to

$$\int_{B(P_1, r_c)} Er \, dr \, dz \tag{4.34}$$

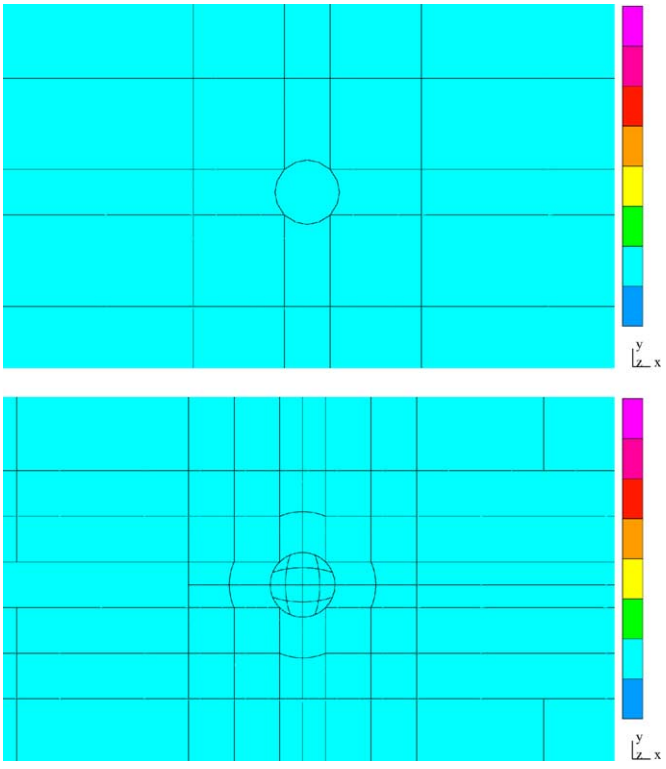

Fig. 11. Energy-based h-adaptivity (above) and goal-oriented h-adaptivity (below), zoom = 1000 towards the receiving antenna.

motivates us to approximate

$$|N(E_{h,p}) - N(E)| = 20\left|\log_{10}\frac{\int_{B(P_1,r_c)} E_{h,p} r\,\mathrm{d}r\,\mathrm{d}z}{\int_{B(P_1,r_c)} Er\,\mathrm{d}r\,\mathrm{d}z}\right| \approx \frac{20}{\ln 10}\left|\frac{\int_{B(P_1,r_c)} E_{h,p} r\,\mathrm{d}r\,\mathrm{d}z - \int_{B(P_1,r_c)} Er\,\mathrm{d}r\,\mathrm{d}z}{\int_{B(P_1,r_c)} Er\,\mathrm{d}r\,\mathrm{d}z}\right|. \tag{4.35}$$

We see that due to the 'linearity' of function $\log_{10}(y)$ at $y = 1$, the minimization of the error in $N(E)$ translates into the minimization of the error in the quantity

$$L(E) = \int_{B(P_1,r_c)} Er\,\mathrm{d}r\,\mathrm{d}z. \tag{4.36}$$

Thus, the goal of our computation is the integral of E_r over the receiving antenna $B(P_1, r_c)$. The constant 20/ln(10) is used in the stopping criterion for the adaptive algorithm only (Figs. 10–13).

4.2. h-adaptivity results

Let us show a few results (resulting optimal meshes in the neighborhood of the antennas) of both the energy-based and goal-oriented *h*-adaptive schemes. All schemes start from the same coarse initial mesh consisting of second-order elements. Similarly as in Section 3.4. the scale on the right-hand side represents the order of polynomial approximation. Energy-based and goal-oriented *h*-adaptivity are performed using second order elements only.

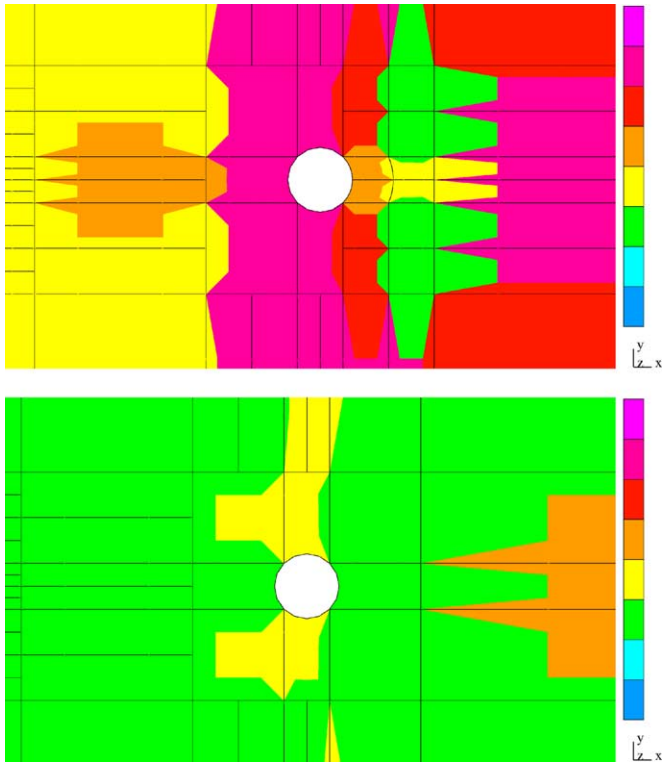

Fig. 12. Energy-based *hp*-adaptivity (above) and goal-oriented *hp*-adaptivity (below), zoom = 1000 towards the emitting antenna.

Fig. 14 shows the history of the relative error in goal (i.e. in the non-linear quantity (4.31)) for all four tested approaches. The unknown exact solution to the radiation problem is replaced by the corresponding fine mesh solution for the error evaluation. The x-axis represents the number of degrees of freedom.

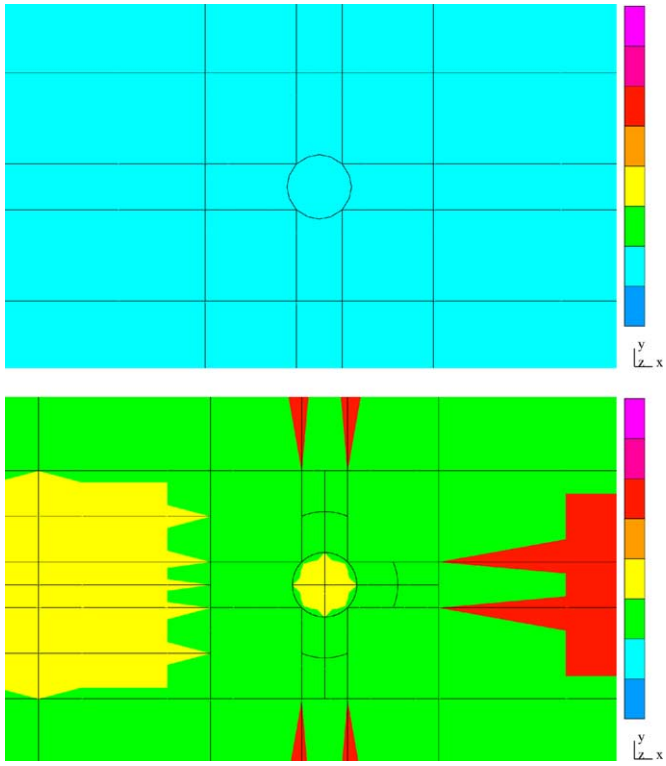

Fig. 13. Energy-based *hp*-adaptivity (above) and goal-oriented *hp*-adaptivity (below), zoom = 1000 towards the receiving antenna.

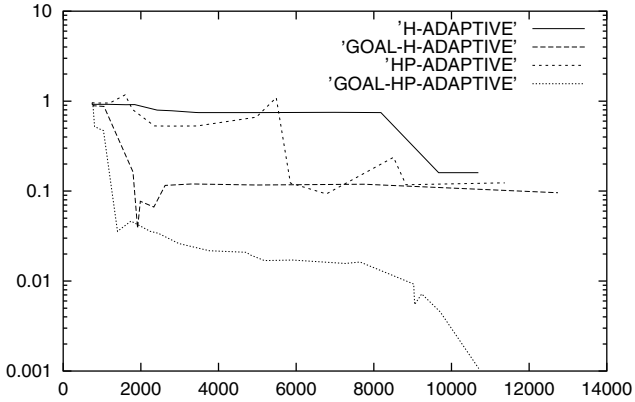

Fig. 14. Relative error in goal (*h*-adaptivity with quadratic elements only, *hp*-adaptivity with initially quadratic elements).

The presented results show a dramatic difference between the energy and goal driven adaptivity. The corresponding meshes are essentially different, and the goal-oriented adaptivity delivers results that are at least an order of magnitude better.

Concerning the difference between the goal-driven *h*- and *hp*-adaptive schemes, we can risk a statement that, within the investigated range of problem size, *hp*-adaptivity delivers results that are an order of magnitude better than those produced by *h*-adaptivity only.

For all investigated strategies, the (estimated or computed) error in goal does not decrease monotonically, especially for energy driven schemes.

Finally, we would like to emphasize that for the antenna problem, that has motivated this research project, the goal-oriented *hp*-adaptive scheme has delivered an outstanding 1/10 of a percent accuracy (on the decibel scale) which seems to be more than satisfactory from the practical point of view.

5. Conclusions

The aim of this study was to bring together the advantages of two powerful tools of numerical mathematics, the *hp*-adaptivity and the goal-oriented adaptivity, into a fully automatic goal-oriented *hp*-adaptive strategy for elliptic problems. We have extended an existing fully automatic *h*-adaptive strategy in energy norm by introducing the solution of the dual problem and applying it to the mesh optimization algorithm based on the minimization of the projection-based *hp*-interpolation error of reference solutions to both the primal and the dual problems.

The numerical results presented in the last two sections demonstrate the advantages of this approach with respect to both the goal-oriented *h*-adaptive strategy and *hp*-adaptive strategy in energy norm.

However, as often the case with 2D computations, this work stands as merely a proof of concept. The ultimate challenge we are heading for is the fully automatic goal-oriented *hp*-adaptivity in three spatial dimensions, on which we hope to report soon.

Acknowledgements

The first author was supported by a TICAM postdoctoral fellowship award and Grant agency of the Czech Republic under the project GP102/01/D114. The second author was sponsored by the Air Force under contract F49620-98-1-0255.

References

[1] M. Ainsworth, B. Senior, Aspects of an *hp*-adaptive finite element method: adaptive strategy, conforming approximation and efficient solvers, Comput. Methods Appl. Math. Engrg. 150 (1997) 65–87.

[2] I. Babuška, T. Strouboulis, K. Copps, S.K. Gangaraj, C.S. Upadhyay, A-Posteriori Error Estimation for Finite Element and Generalized Finite Element Method, TICAM Report 98-01, The University of Texas at Austin, 1998.

[3] R. Becker, R. Rannacher, Weighted A-Posteriori Error Control in FE Method, ENUMATH-95, Paris, September 1995.

[4] R. Becker, R. Rannacher, A feedback approach to error control in finite elements methods: basic analysis and examples, East–West J. Numer. Math. 4 (1996) 237–264.

[5] F. Cirak, E. Ramm, A-posteriori error estimation and adaptivity for linear elasticity using the reciprocal theorem, Comput. Methods Appl. Mech. Engrg. 156 (1998) 351–362.

[6] L. Demkowicz, J.T. Oden, W. Rachowicz, O. Hardy, Toward a universal *hp*-adaptive finite element strategy. Part 1: Constrained approximation and data structure, Comput. Methods Appl. Math. Engrg. 77 (1989) 79–112.

[7] L. Demkowicz, I. Babuška, Optimal *p* Interpolation Error Estimates for Edge Finite Elements of Variable Order in 2D, TIC AM Report 01-11.

[8] L. Demkowicz, W. Rachowicz, Ph. Devloo, A fully automatic *hp*-adaptivity, J. Sci. Comput. 17 (1-3) (2002) 127–155.
[9] L. Demkowicz, Asymptotic convergence in finite and boundary element methods. Part 1: Theoretical results, Comput. Math. Appl. 27 (12) (1994) 69–84.
[10] P. Houston, B. Senior, E. Süli, Sobolev regularity estimation for *hp*-adaptive finite element methods, in: F. Brezzi, A. Buffa, S. Corsaro, A. Murli (Eds.), Numerical Mathematics and Advanced Applications, Springer-Verlag, Berlin, 2003, pp. 619–644.
[11] J.R. Lovell, Finite Element Methods in Resistivity Logging, Delft University of Technology, 1993, pp. 38–45.
[12] J.T. Oden, S. Prudhomme, Goal-oriented error estimation and adaptivity for the finite element method, Comput. Math. Appl. 41 (2001) 735–756.
[13] M. Paraschivoiu, A.T. Patera, A hierarchical duality approach to bounds for the outputs of partial differential equations, Comput. Methods Appl. Mech. Engrg. 158 (1998) 389–407.
[14] J. Peraire, A.T. Patera, Bounds for linear-functional outputs of coercive partial differential equations: local indicators and adaptive refinement, in: P. Ladevèze, J.T. Oden (Eds.), Advances in Adaptive Computational Methods in Mechanics, Elsevier, Amsterdam, 1998, pp. 199–215.
[15] W. Rachowicz, J.T. Oden, L. Demkowicz, Toward a universal *hp*-adaptive finite element strategy. Part 3: Design of *hp* meshes, Comput. Methods Appl. Math. Engrg. 77 (2) (1989) 181–212.
[16] W. Rachowicz, L. Demkowicz, An *hp*-adaptive finite element method for electromagnetics. Part II: A 3D implementation, Int. J. Numer. Methods Engrg. 53 (2002) 147–180.
[17] R. Rannacher, F.T. Stuttmeier, A-posteriori error control in finite element methods via duality techniques: application to perfect plasticity, Comput. Mech. 21 (1998) 123–133.
[18] C. Schwab, *p*- and *hp*-Finite Element Methods, Clarendon Press, Oxford, 1998.
[19] P. Šolín, K. Segeth, I. Doležel, Higher-Order Finite Element Methods, Chapman & Hall/CRC Press, Boca Raton, 2003.